Electrocatalysis (2015) 6:229–236
DOI 10.1007/s12678-014-0237-7

High-Throughput Screening for Acid-Stable Oxygen Evolution Electrocatalysts in the (Mn–Co–Ta–Sb)O_x Composition Space

Aniketa Shinde · Ryan J. R. Jones · Dan Guevarra · Slobodan Mitrovic · Natalie Becerra-Stasiewicz · Joel A. Haber · Jian Jin · John M. Gregoire

Published online: 7 November 2014

Abstract Solar generation of fuel is a promising future energy technology, and strong acidic conditions are highly desirable for integrated solar hydrogen generators. In particular, water splitting near pH 0 is attractive due to the availability of high theoretical efficiency, high performance hydrogen evolution catalysts, and robust ion exchange membranes. The lack of a stable, earth-abundant oxygen evolution catalyst inhibits deployment of this technology, and development of such a material is hampered by the strong anti-correlation between electrochemical stability and catalytic activity of non-precious metal oxides. High-throughput screening of mixed metal oxides offers a promising route to the identification of new stable catalysts and requires careful design of experiments to combine the concepts of rapid experimentation and long-term stability. By combining serial and parallel measurement techniques, we have created a high-throughput platform to assess the catalytic activity of material libraries in the as-prepared state and after 2 h of operation. By screening the entire (Mn–Co–Ta–Sb)O_x composition space, we observe that the compositions with highest initial activity comprised cobalt and manganese oxides, but combinations with antimony and tantalum offer improved stability. By combining the desired properties of catalytic activity and stability, the optimal composition regions are readily identified, demonstrating the success and fidelity of this novel high-throughput screening platform.

A. Shinde · R. J. R. Jones · D. Guevarra · S. Mitrovic · N. Becerra-Stasiewicz · J. A. Haber · J. M. Gregoire (✉)
Joint Center for Artificial Photosynthesis, California Institute of Technology, Pasadena, CA 91125, USA
e-mail: gregoire@caltech.edu

J. Jin
Engineering Division and Joint Center for Artificial Photosynthesis, Berkeley National Laboratory, Berkeley, CA 94720, USA

Keywords Solar fuels · Water splitting · High throughput · Oxygen evolution · Electrochemical stability

Introduction

The efficient photoelectrochemical synthesis of clean hydrogen fuel is an attractive renewable energy technology. Feasible large-scale deployment of this type of system requires the discovery of improved electrocatalysts containing only earth-abundant elements [1–3]. In particular, the 4-electron oxygen evolution reaction (OER) is kinetically slow and improved catalysts are required for artificial photosynthesis and electrolysis of hydrogen [2]. An important issue in electrolysis system design is the separation of the H_2 and O_2 reaction products to avoid creating explosive gas mixtures. Incorporation of a cation or anion exchange membrane prevents the convective and mitigates the diffusive crossover of products between the cathode chamber where the H_2 is evolved and the anode chamber where O_2 is evolved. Due to the very small transference number of active species in ion exchange membranes under near-neutral pH conditions, acidic or alkaline solutions (e.g., 1 M H_2SO_4 or 1 M KOH) are desirable to minimize the transport loss through the membrane separator [4]. Moreover, modeling and experimental demonstrations have shown that significant voltage losses occur in the bulk of the electrolyte under operation at near-neutral pH in buffered solutions, which result from pH gradients that form at the surface of the photoelectrodes [5]. Thus, conventional electrolyzer or fuel cell systems involve the use of acidic or alkaline electrolytes along with a suitable cation- or anion-exchange membrane to minimize concentration overpotentials and resistive loss in the solution and membrane. The commercial availability of cation exchange membranes with proven performance and durability makes acidic environments particularly attractive for electrolysis of H_2. Additionally, several

non-precious metal hydrogen evolution electrocatalysts have shown great promise for high activity and stability in acid [1, 6]. The identification of a stable, earth-abundant oxygen evolution catalyst would be an enabling discovery for the deployment of electrolysis and photoelectrolysis technology.

Mixed metal oxides offer promise for improved catalysis and stability due to the existence of a wide variety of alloys and compounds. Only a minute fraction of the known materials have been tested for OER catalysis and computational efforts indicate that only a small fraction of materials have been experimentally observed [7]. An important new computational tool provides calculations of electrochemical stability for compounds, particularly in high-order composition spaces [8]. While these thermodynamic calculations can guide the search for electrochemically stable materials, electrochemical stability is often attained through a variety of kinetic effects, in particular the formation of passivation layers on metal electrodes [9, 10]. As a result, the search for new stable OER catalysts involves a vast material space of interest that combines high-order composition spaces with an extensive material processing space. High-throughput experimentation offers an efficient means for exploring new materials, but known properties of elemental metal oxides indicate that the vast majority of mixed non-precious metal oxides will quickly corrode in the operational conditions for OER electrocatalysis in acid.

Previous studies of OER electrocatalysts that utilized high-throughput experimentation involved quick electrochemical measurements of precious metal systems in mildly acidic environments (pH near 3) [11–13]. The common method of parallel, high-throughput screening utilizes a fluorescence imaging system [14] in which a material library is immersed in an electrolyte solution near or above pH 3. By applying a bias across the entire library at a chosen OER overpotential, active catalysts are identified by a pH-sensitive fluorescence indicator that relies upon the local accumulation of protons produced by the OER. Rapid identification of the active compositions results from imaging local changes in pH over a measurement time on the order of 10 s. However, the technique cannot be employed at pH 0 or for long-duration experiments. For non-precious metal oxides, many corrosion processes will also produce protons, leading to false-positive signals using this technique.

While distinguishing corrosion from OER catalysts is challenging for short-duration experiments, a simple charge conservation argument can be exploited to interpret electrochemical current from catalysts operated over longer periods. The maximum charge a catalyst sample can yield as a result of corrosion can be estimated from the moles of metal in the sample and the number of electrons generated per metal atom (assumed to be an average of 1 for simplicity). The ratio of this maximum corrosion charge to the total charge passed during a measurement provides an estimate for the upper limit on the branching ratio for corrosion, motivating the development of long-duration screening methods. To balance the requirements for high throughput, long-term durability, and direct measurement of catalytic activity, we have developed a combination of parallel and serial screening measurements. The long-duration stability measurements are performed in a newly developed parallel electrochemical treatment system whose design and operation were developed through extensive engineering and modeling.

Electrochemical stability in acid has been studied primarily for electrocatalysts of the oxygen reduction reaction (ORR), which operate at considerably lower potentials than OER electrocatalysts [15, 16]. The vast majority of ORR systems are alloys of precious metals, most notably Pt alloys [17, 18], although some non-precious metal oxides have been studied as catalyst supports [15]. For OER in acid, catalyst development efforts include mixed oxides of precious metals to stabilize RuO_2 [19] and studies of mixed metal oxides combining Ir or Ru with non-precious metal oxides, such as those of Sn [20, 21] and Ta [22, 23]. Kadakia et al. demonstrated a highly active OER catalyst with substantially lowered concentration of precious metal by alloying IrO_2 with NbO_2 and SnO_2 [24]. A recent study evaluating a series of metal oxides under well-controlled conditions showed that under acidic conditions, IrO_x was the only OER electrocatalyst that exhibited catalytic activity with a 2-h stability under operational conditions [25]. The report presented numerous metal (hydr)oxides that catalyze OER in alkaline conditions, such as (hydr)oxides of Mn, Fe, Co, and Ni, but all of these proved unstable in acidic conditions. According to Pourbaix diagrams, several metal oxides are stable in acidic conditions at OER potentials, such as oxides of Mo, Sn, and Sb, but these metal oxides do not exhibit appreciable catalytic current at overpotentials below 700 mV. Thus, to identify earth-abundant, stable OER catalysts, we screened composition spaces that include both catalytic, unstable oxides, and non-catalytic, stable oxides with the hypothesis that the stable oxides may thermodynamically or kinetically stabilize a catalytically active material. The $(Mn–Co–Ta–Sb)O_x$ system is one such composition space, and here we show improved performance of the mixed metal oxides compared to the elemental oxides. After operation at approximately 1.8 V vs NHE for 2 h, a wide range of compositions yield a catalytic current of 3 mA cm^{-2} with overpotential below 550 mV, which is unprecedented performance for non-precious metal oxides.

Experimental

Library Synthesis

The pseudo-quaternary $(Mn–Co–Ta–Sb)O_x$ libraries were each deposited as an array of 1771 discrete compositions at

5.0 at.% composition steps [26, 27]. The 1 mm×1 mm composition samples were produced by inkjet printing four separate metal precursor inks containing $Mn(NO_3)_2$, $Co(NO_3)_2$, $TaCl_5$, and $SbCl_3$, respectively. The ethanol-based inks were prepared by a previously described method [28, 29], and contained 1 % Pluronic F127 to affect ink rheology and drying. Each composition was prepared by depositing 3.8 nM of metal onto a 1-mm [2] area of glass substrate with conductive SnO_2:F coating. The inks were dried and the metal precursors converted to oxides by calcination in air at 450 °C.

To elucidate temporal stability characteristics, two identical libraries, A and B, were produced. The 1771 catalyst compositions in both library A and library B were distributed randomly over the grid of sample positions so that any spatial artifacts would not appear as systematic composition trends in the compositional figure of merit (FOM) maps. Library B was subject to electrochemical conditions relevant to OER catalysis for 2 h, as described below, and images of the library were acquired with a commercial photo scanner (Epson Perfection V600 PHOTO) before and after electrochemical exposure.

Library Screening

High-throughput electrochemical experiments were carried out utilizing a novel combination of serial and parallel techniques. Library A was subject to serial measurements to establish the catalytic activity of each composition in the "as-synthesized" state. Library B was first subject to parallel measurements for 2 h in a newly developed parallel electrochemical treatment system that exposed all samples to a simultaneous and uniform electrochemical environment, followed by serial measurements, which establish the catalytic activity of each sample after 2 h of electrochemical exposure. We assert that the difference in catalytic activity between an "as-synthesized" composition (library A) and electrochemically treated composition (library B) relates directly to stability on the 2-h time scale, as described below. In this manuscript, we report catalytic activity, temporal stability, and compositional properties as a function of the intended library compositions. For all experiments, the library plate served as the working electrode for electrochemical measurements, with electrical contact established by placing 0.25″ wide copper tape (McMaster-Carr) around three of the four perimeter edges. An O_2-saturated 1.0 M H_2SO_4(aq) electrolyte solution was used in both serial and parallel instruments.

Scanning Droplet Cell

Serial measurements of OER activity were performed using a previously reported scanning droplet cell (SDC) that established an individual 3-electrode cell for each sample, including the conducting substrate, a capillary Ag/AgCl reference electrode, and a platinum wire counter electrode. The activity of each catalyst composition was characterized using 15 s chronopotentiometry (CP) measurements at 3 mA cm^{-2} (all current densities in this work reference geometric area). The corresponding OER overpotential (η) was used as the FOM for each catalyst sample. The CP measurements of the as-synthesized materials (library A) may include anodic currents from both OER catalysis and sample corrosion. On the other hand, the CP measurements of the post-stability experiment materials (library B) cannot contain substantial contribution from corrosion. If a given composition sample corrodes at a current density of 5 μA cm^{-2} (0.17 % of that used in the CP measurement), then the entire sample would be gone after the 2-h stability experiment. Accordingly, we assert that the 3 mA cm^{-2} SDC experiments on library B (post-stability experiment) provide robust measurement of the OER catalyst activity of each material, and that these catalysts have reached some level of equilibration during the 2-h exposure to acidic OER conditions.

The SDC measurements exhibit some experimental noise, and to better visualize the systematic composition trends, a simple smoothing algorithm was applied to the composition space FOM plots. For a select composition, the reported FOM is the average FOM over the set of samples formed by taking the select composition and symmetric pairs of composition neighbors. This is done such that the average composition over this set of symmetric samples is equal to the selected composition. For pseudo-unary, pseudo-binary, pseudo-ternary, and pseudo-quaternary compositions, the number of samples in the symmetric set is 1, 3, 7, and 13, respectively. For each set of symmetric FOM values, any outlier FOM value beyond 2 standard deviations of the mean FOM was disregarded.

Parallel Electrochemical Treatment System

Stability experiments on library B compositions were performed using a newly developed parallel electrochemical treatment system, a schematic of which is illustrated in Fig. 1. It consists of three polymethyl-methacrylic (McMaster-Carr) pieces stacked on top of one another and separated by a Nafion membrane (N117, IonPower Inc.) that demarcates the anolyte and catholyte chambers. This stacked assembly is mechanically sealed to the library substrate in such a way to provide solution contact to the inner area of the substrate containing the composition library, while avoiding solution contact to the outer perimeter of the substrate and the electrical connection (Cu tape). The library substrate serves as the working electrode, and a planar mesh counter electrode is suspended parallel to the working electrode, in the catholyte chamber, at a distance of 7–10 mm. A reference electrode (Ag/AgCl, CH Instruments) is placed in the anolyte chamber less than 5 mm from the plane of the working electrode surface to establish pseudo 3-electrode measurements.

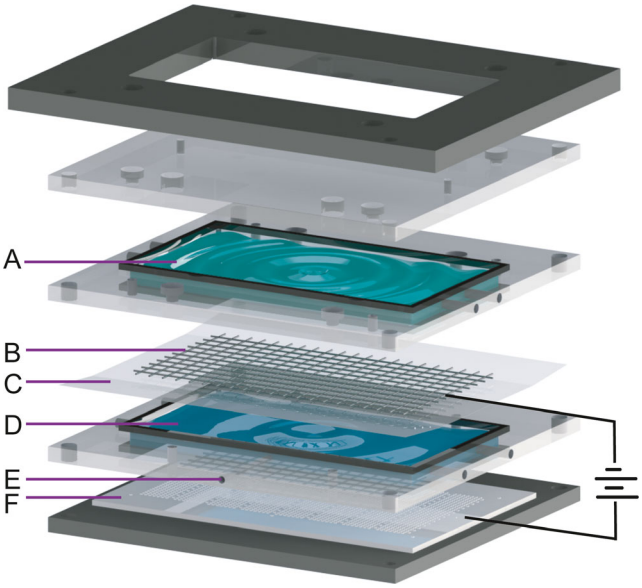

Fig. 1 An illustration of the parallel electrochemical treatment system: **a** catholyte, **b** planar counter electrode, **c** Nafion membrane, **d** anolyte, **e** reference electrode port, and **f** working electrode (library substrate)

Using the assembly shown in Fig. 1, the electrochemical treatment of library B was performed in 1.0 M H_2SO_4(aq) electrolyte, which was introduced into the catholyte and anolyte chambers through separate recirculation systems that operated continuously throughout the experiment. In particular, the anolyte solution was recirculated at 10 mL min^{-1} with a 1 L reservoir to ensure that the concentration of metal remained below 7 μM even if the entire library dissolved into solution. After preparation of the cell, a potentiostat (Gamry Reference 600) was used to perform a 2-h CP measurement at 25 mA, which corresponds to an average current density of 0.26 mA cm^{-2} for the wetted electrode area and 1.4 mA cm^{-2} for the composition samples. This total current was chosen to provide a relevant operational anodic potential of approximately 600 mV overpotential for the OER. The experiment was performed at constant current instead of constant potential, because we found that limiting the current was important to avoid spatial variations in the working electrode potential, which arise from ohmic losses through the SnO_2:F conducting plane. After the 2-h experiment, the substrate was immediately removed and excess solution was cleared from the surface. The library was then imaged and transferred to the SDC for serial catalytic performance measurements.

Photoelectron Spectroscopy

X-ray photoelectron spectroscopy (XPS) data were collected using a Kratos Axis NOVA (Kratos Analytical, Manchester, UK) with excitation from a monochromatized Al K(alpha) source at 1486.6 eV. The measurement area was approximately 0.8 mm in diameter and centered on the 1-mm [2] sample area with a take-off angle to the detector of 35.5°. Pressure in the analysis chamber was low 10^{-9} Torr during the measurement. Survey scans were collected at pass energy 160 eV, and high-resolution scans at pass energy 20 eV. Charge neutralization was not applied, but no evidence of sample charging was observed.

Results and Discussion

Catalytic Activity and Stability

Two duplicate (Mn–Co–Ta–Sb)O_x libraries were prepared for measuring the activity and stability of OER catalysis in pH 0. For library A, SDC measurements were performed to establish the catalytic activity of the as-synthesized compositions and the results are shown in Fig. 2. Library B was screened for stability with a parallel 2-h CP measurement at 25 mA, and the measured voltage is shown in Fig. 3a. Figure 3b, c shows

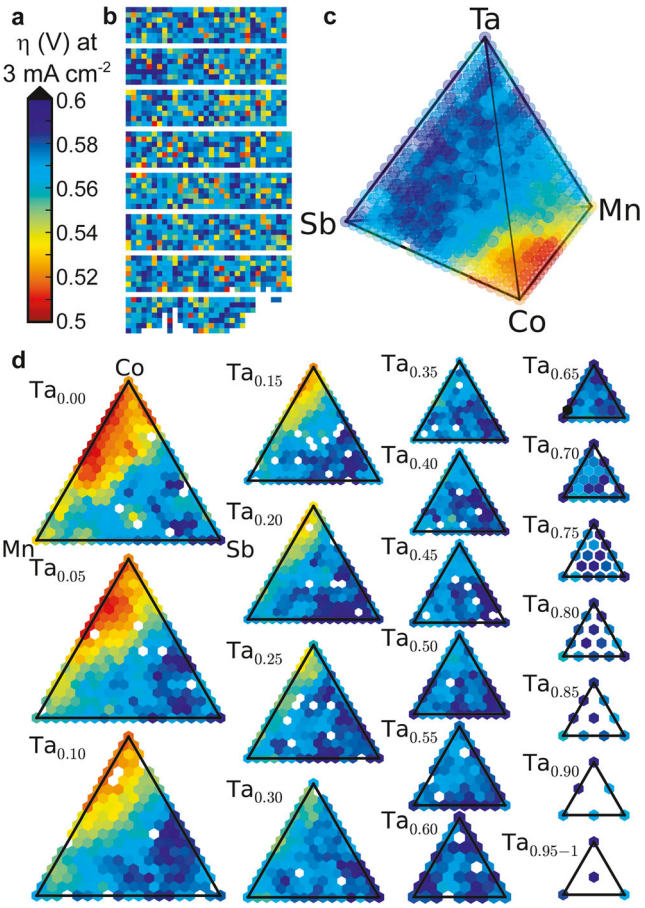

Fig. 2 Catalytic performance of library A (as-synthesized) obtained from scanning droplet cell measurements in 1 M H_2SO_4 at 3 mA cm^{-2}. The color scale (**a**) for overpotential (η) applies to all three mappings: **b** spatial map over the library plate, **c** tetrahedron plot of the quaternary composition space, and **d** pseudo-ternary composition plots which are a deconstruction of the tetrahedron

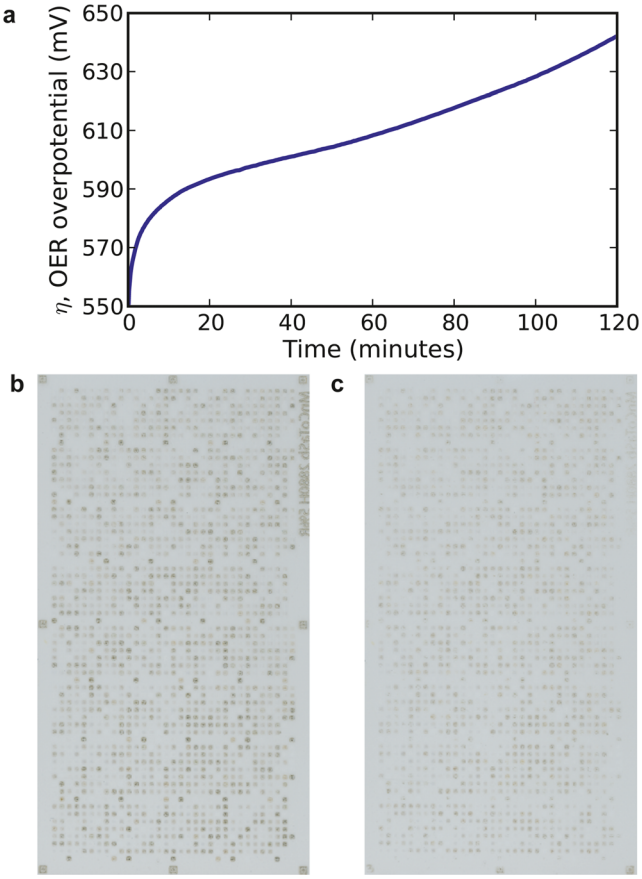

Fig. 3 **a** Measured potential (CP) for the library B plate during the stability experiment at 25 mA in 1 M H_2SO_4. Scanned images of the (Mn–Co–Ta–Sb)O_x library are shown before (**b**) and after (**c**) the stability experiment

photo-scanned images of library B before and after the CP stability experiment, respectively. The increasing overpotential during the 2 h CP measurement is likely due to a combination of effects including deactivation of OER catalysts, decay of corrosion currents due to kinetic limitations such as formation of a surface passivation layer, and complete corrosion of some samples. Detailed interpretation of the CP trace is limited by the inclusion of 1771 unique compositions in the experiment and the parallel nature of this high-throughput method, but additional information can be discerned by comparison of the scanned images before and after the stability experiment. On average, the as-synthesized materials are darker than the post-stability experiment materials, and closer inspection reveals that many compositions were mostly or completely etched by the stability experiment. It is important to note that for compositions in which electrochemical corrosion occurs, the measured overpotential in the SDC experiments on as-synthesized materials (library A) may include both OER electrocatalysis and corrosion, effectively increasing the probability of false-positive catalyst identification. The need to mitigate the likelihood of false positives due to corrosion currents in catalyst screening is a prime motivator for introducing the parallel electrochemical treatment system to the high-throughput catalyst evaluation platform.

Figure 4 shows the catalytic performance of library B after the stability experiment using the same false-color scale (for η at 3 mA cm^{-2}) as Fig. 2, so that these figures can be directly compared. Most SDC CP traces exhibited a voltage transient lasting approximately 5 s, with the voltage signal reaching quasi-equilibrium at the end of the 15 s. Due to the random spatial distribution of the 1771 compositions on each substrate, no systematic trends are observed in the position maps of the FOM (Figs. 2b and 4b). Composition maps of the FOM (Figs. 2c and 4c) are shown as tetrahedron plots of the quaternary composition space and a series of pseudo-ternary composition plots (Figs. 2d and 4d), which are 5 at.% slices along the Ta direction of the composition tetrahedron. For each library, a few percent of the SDC measurements were corrupted, resulting in missing composition measurements in the spatial position maps, but due to the random spatial distribution of samples, the corresponding sparse holes in the composition maps do not preclude the identification of

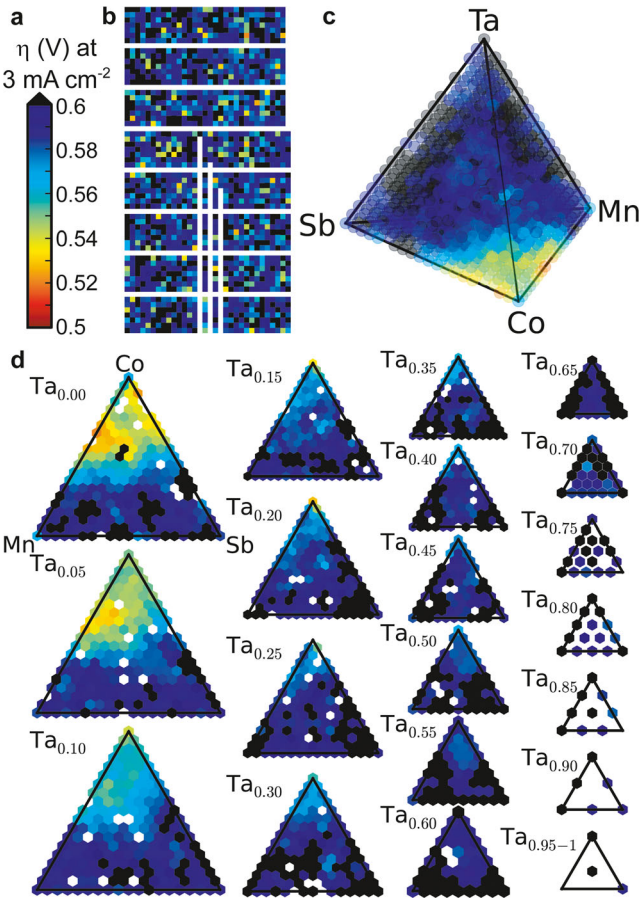

Fig. 4 Catalytic performance of library B (post-stability experiment) obtained from scanning droplet cell measurements in 1 M H_2SO_4 at 3 mA cm^{-2}. The color scale (**a**) for overpotential (η) applies to all three mappings: **b** spatial map over the library plate, **c** tetrahedron plot of the quaternary composition space, and **d** pseudo-ternary composition plots which are a deconstruction of the tetrahedron

composition trends. It is worth noting that the horizontal rows without samples in Figs. 2b and 4b are substrate positions reserved for reference measurements.

The as-synthesized OER catalyst compositions with best initial activity are near $Mn_{0.3}Co_{0.7}O_x$, and in the surrounding composition region including most of the Mn–Co compositions, with up to 25 at.% Ta and up to 30 at.% Sb. Considering Fig. 2 (library A) to be a measurement of initial OER overpotential ($\eta_{t=0h}$) and Fig. 4 (library B) to be a corresponding measurement after 2 h of catalysis ($\eta_{t=2h}$), compositions for which $\eta_{t=0h}$ and $\eta_{t=2h}$ are approximately equal ($\eta_{t=2h}-\eta_{t=0h}\approx 0$) are promising acid-stable OER catalysts. The measurements of $\eta_{t=2h}$ show that the catalysts with the very best $\eta_{t=0h}$ values experience some deactivation during the stability experiment. Some catalysts on the edge of the aforementioned composition region exhibit approximately the same $\eta_{t=0h}$ and $\eta_{t=2h}$ values, most notably compositions near $Mn_{0.3}Co_{0.4}Sb_{0.3}O_x$, which exhibited slightly lower overpotentials after the stability experiment. An argument can be made for using $\eta_{t=2h}$ to identify the best catalysts, but for the purpose of predicting which compositions may be stable catalysts for much longer durations, it is prudent to consider the change in overpotential.

Sample Down-Selection

An important utility of high throughput experiments is the capability to identify composition regions that should be studied more closely with traditional (low-throughput) techniques. Such down-selection can be readily performed using the data in Figs. 2 and 4 with a variety of techniques. To combine the desirable properties of low overpotential and high stability, down-selection criteria $\eta_{t=2h}<0.57$ V and $\eta_{t=2h}-\eta_{t=0h}<0.02$ V was applied. These criteria identified 83 compositions from the initial set of 1771 compositions, which are shown in Fig. 5. The selected samples included a series of compositions near the pseudo-binary line $Co_{1-z}Ta_zO_x$ with z varying from 0.15 to 0.3. Most of the compositions are in the (Co–Mn–Sb)O_x space or neighboring compositions with 5 % Ta. In this cluster of select compositions, Ta offers no clear benefit to performance, and the representative compositions are binary and ternary mixtures of Co with Mn and/or Sb. The Co concentrations are mostly within the 50–90 % range, and the compositions span a wide range of Mn:Sb ratios. The down-selected compositions are clustered in composition space, indicating that representative compositions should be studied further and demonstrating the utility of the high-throughput screening platform.

XPS Measurements

Composition characterization is desirable before and after the stability experiment to observe composition changes, particularly at the surface or near-surface of a sample. It is worth noting that the solution drop from a SDC experiment leaves a

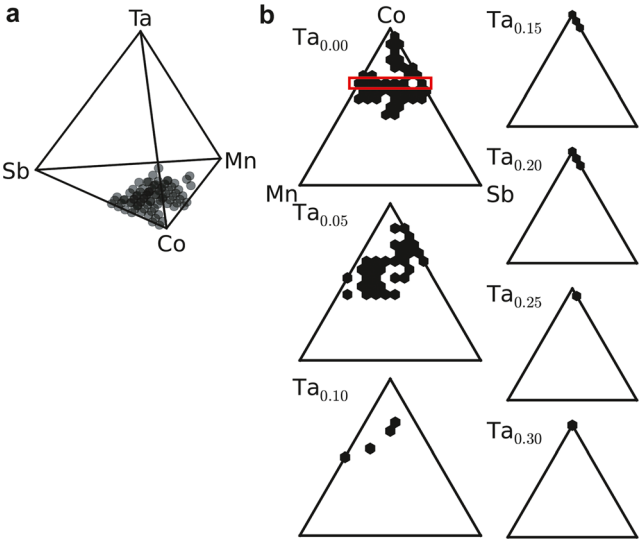

Fig. 5 Select compositions meeting criteria of (i) less than 0.02 V change in η over a 2-h OER operation and (ii) $\eta<0.57$ V for OER catalysis after the 2-h stability experiment. The *red rectangle* highlights a series of compositions characterized by X-ray photoelectron spectroscopy

thin layer of solution on each sample as it rasters across the library for approximately 6 h. During this time, the thin layer of solution dries and the pH of the surface solution is not controlled. The near-surface compositions may be affected by this uncontrolled chemical history, precluding analysis of the active catalyst material post-SDC measurement. Since both libraries A and B underwent SDC experiments, a duplicate library (library C) was synthesized to characterize changes in composition during exposure to the 2-h stability experiment. To mimic the electrochemical history of library B, the full (Co–Mn–Sb–Ta)O_x composition library was deposited and operated for 2 h in the parallel electrochemical treatment system using the same 25-mA CP measurement, producing results similar to those in Fig. 3a. Collection of XPS spectra on all 1771 samples was impractical, so compositions for characterization were selected with consideration of the composition trends in Figs. 2, 3, 4 and 5. Figure 5 shows this series of eight selected compositions along the pseudo-binary line $Co_{0.65}Mn_{0.35-y}Sb_yO_x$, outlined by a red rectangle. XPS characterization of the eight selected compositions in library C was performed first on the as-synthesized materials, and then again after the 2-h stability experiment, as shown in Fig. 6.

High-resolution spectra of Co, Mn, and Sb core levels are shown in Fig. 6, revealing important trends in electrochemically modified composition with respect to the composition parameter y. The Co and Mn signals of the as-synthesized materials are commensurate with the intended compositions, and the signals from these elements are much lower in the post-stability experiments, indicating significant electrochemical leaching. The intensity of the Sb signal is relatively unaffected by the stability experiment. Because the Sb 3*d* 5/2 peak strongly overlaps with O 1*s* peaks, and there appear to

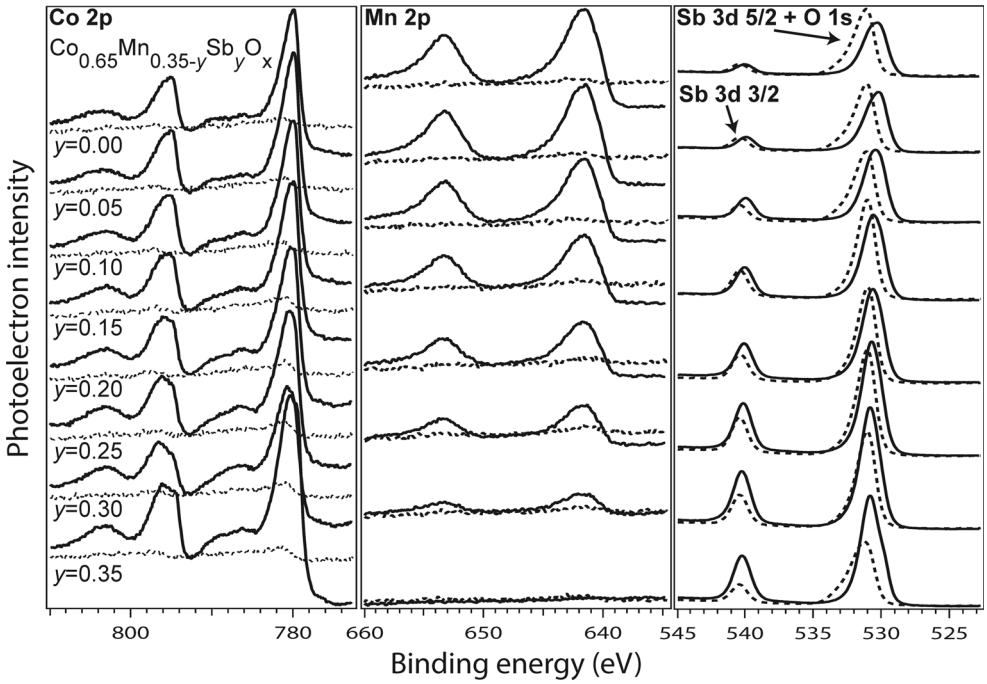

Fig. 6 Core-level X-ray photoelectron spectroscopy data for the eight samples along composition line $Co_{0.65}Mn_{0.35-y}Sb_yO_x$ in library C. The as-synthesized signal (*solid line*) and signal after a 2-h stability experiment (*dashed line*) are shown for each core level and each composition

be multiple O 1*s* peaks, the position of the Sb 3*d* 3/2 peak provides the best indication of any electrochemistry-induced peak shifting. The slight shift to higher binding energy is commensurate with a change in the Sb formal oxidation state from +3 as-synthesized to +5 after electrochemistry.

The Sb signals also reveal a significant issue, in particular that the as-synthesized $y=0$ sample exhibits a small, but finite, signal. It is important to note that the signal is present in both the as-synthesized and post-electrochemistry material, and thus indicates that the sample was contaminated with Sb during the library synthesis process and not during the electrochemical testing process. As part of synthesis quality control, energy dispersive X-ray spectroscopy and xXray fluorescence measurements were performed to confirm that the library samples contain the intended compositions. However, the presence of Sb was not observable by these techniques due to the strong overlap with the large Sn signal from the SnO_2:F coating on the substrate. After extensive XPS measurements and further diagnostics, we have concluded that the inkjet printer malfunctioned and released small amounts of the Sb ink into all samples and in fact the entire library plate during the synthesis of libraries A, B, and C. For Sb-rich samples, this artifact is inconsequential, and for low-Sb compositions the synthesized materials contain more Sb than intended by approximately 3 at.%. The only substantial impact this artifact has on the results of Figs. 2, 3, 4 and 5 is that the samples on the (Co–Mn)O_x binary line, which contain two compositions that meet the down-selection criteria, actually contain a small concentration of Sb. Given the electrochemical stability of neighboring compositions, and the known instability of Co and Mn under these electrochemical conditions, this small amount of Sb may be important.

The inclusion of Sb, and to some extent Ta, in the (Co–Mn)O_x catalysts appears to be beneficial, though it is important to note that the Sb-rich and Ta-rich compositions exhibit poor OER activity (comparable to the SnO_2:F underlayer). Figure 6 indicates that the $Co_{0.65}Mn_{0.35-y}Sb_yO_x$ compositions become more Sb-rich during exposure to the electrochemical stability experiment, but the resulting (Sb-rich) composition(s) can be found elsewhere in the composition library, and Figs. 2 and 4 show that their OER activity is lower. These observations may be explained by several phenomena including a substantial increase in surface area of the Sb-rich compositions, the formation of a novel morphology that increases the specific activity of surface Sb, or the formation of a Sb-rich surface layer whose catalytic properties are affected by a Sb-poor sublayer. These phenomena have been observed in previous high-throughput [30] and directed studies [31, 32] in which the as-synthesized material contains both stable and unstable elements. The SnO_2:F support layer may also play a role in the catalysis. The high-throughput discovery and characterization of this composition space has identified a composition region that merits a more detailed investigation to elucidate the chemical and physical properties of these catalytic materials.

Conclusions

The discovery of non-precious metal catalysts for efficient solar fuel generation that are stable at pH 0 under OER conditions is a daunting challenge that stimulates novel research methodologies. Simple material design principles, such as mixing stable metal oxides and common metal oxide catalysts, produce vast

composition spaces to be explored and motivate the application of high-throughput experimentation. Evaluating electrocatalysts for stability under OER conditions at pH 0 is particularly challenging high-throughput measurement, due to the long experiment duration required to demonstrate that OER catalysis occurs at a substantially larger rate than corrosion. The fact that a majority of non-precious mixed metal oxides will corrode under these conditions creates additional challenges related to contamination of the electrochemical instrument and cross-contamination of catalyst material. To address these issues, we developed a new instrument and protocol for high-throughput screening that assesses the catalytic activity and 2-h stability of mixed metal oxides under OER conditions at pH 0. The screen is applied to 1771 compositions covering the entire (Co–Mn–Sb–Ta)O_x composition space in 5 at.% intervals. While Co and Mn-rich compositions are the most active in the as-synthesized library, compositions containing Sb and Ta are also highly active and relatively stable after 2 h of operation. Using down-selection criteria that require both high catalytic activity and long-term stability, the composition regions for further exploration were identified. Initial characterization of the mixed metal oxides indicate that while Co and Mn seem to play an important role in OER catalysis, their concentration in the near-surface of the operated OER catalysts is quite small, warranting further investigation of their role in the excellent performance of these materials.

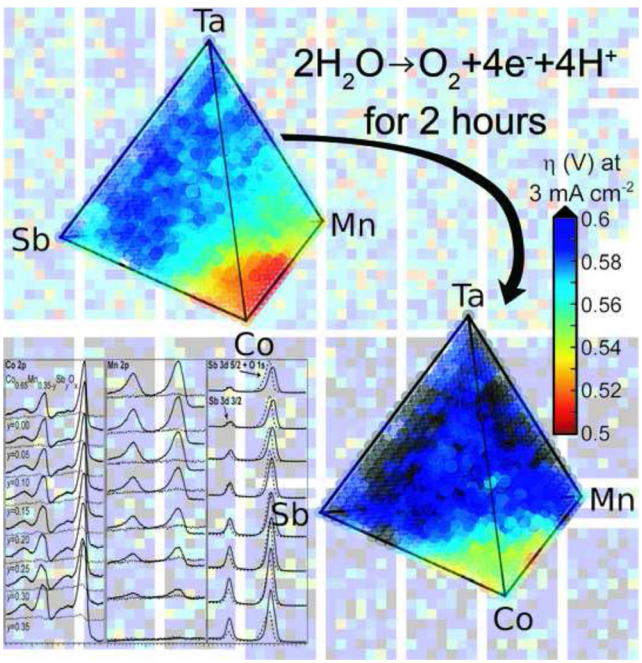

Acknowledgments This manuscript is based upon work performed by the Joint Center for Artificial Photosynthesis, a DOE Energy Innovation Hub, supported through the Office of Science of the U.S. Department of Energy (Award No. DE-SC0004993). The authors thank Dr. Chengxiang Xiang for assistance with establishing the electrochemical treatment system and Dr. Manuel Soriaga for the illuminating discussions.

References

1. M.G. Walter, E.L. Warren, J.R. McKone, S.W. Boettcher, Q.X. Mi, E.A. Santori, N.S. Lewis, Chem. Rev. **110**, 6446 (2010)
2. T.R. Cook, D.K. Dogutan, S.Y. Reece, Y. Surendranath, T.S. Teets, D.G. Nocera, Chem. Rev. **110**, 6474 (2010)
3. J. Suntivich, K.J. May, H.A. Gasteiger, J.B. Goodenough, Y. Shao-Horn, Science **334**, 1383 (2011)
4. Bard, A. J.; Faulkner, L. R. *Electrochemical methods: fundamentals and applications*; (Wiley, 2000)
5. J. Jin, K. Walczak, M.R. Singh, C. Karp, N.S. Lewis, C. Xiang, Energ Environ Sci **7**, 2504–2517 (2014)
6. E. Navarro-Flores, Z. Chong, S. Omanovic, J. Mol. Catal. A Chem. **226**, 179 (2005)
7. S. Curtarolo, G.L.W. Hart, M.B. Nardelli, N. Mingo, S. Sanvito, O. Levy, Nat. Mater. **12**, 191 (2013)
8. K.A. Persson, B. Waldwick, P. Lazic, G. Ceder, Phys Riew B **85**, 235438 (2012)
9. V. Maurice, P. Marcus, Electrochim. Acta **84**, 129 (2012)
10. J. Snyder, J. Erlebacher, J. Electrochem. Soc. **157**, C125 (2010)
11. G. Chen, S.R. Bare, T.E. Mallouk, J. Electrochem. Soc. **149**, A1092 (2002)
12. A.G. Dokoutchaev, F. Abdelrazzaq, M.E. Thompson, J. Willson, C. Chang, A. Bocarsly, Chem. Mater. **14**, 3343 (2002)
13. D. Seley, K. Ayers, B.A. Parkinson, ACS Comb. Sci. **15**, 82 (2013)
14. E. Reddington, A. Sapienza, B. Gurau, R. Viswanathan, S. Sarangapani, E.S. Smotkin, T.E. Mallouk, Science **280**, 1735 (1998)
15. Z. Zhang, J. Liu, J. Gu, L. Su, L. Cheng, Energ. Environ. Sci. **7**, 2535 (2014)
16. L. Su, W. Jia, C.-M. Li, Y. Lei, ChemSusChem **7**, 361 (2014)
17. A. Bonakdarpour, R. Löbel, S. Sheng, T.L. Monchesky, J.R. Dahn, J. Electrochem. Soc. **153**, A2304 (2006)
18. A. Bonakdarpour, K. Stevens, G.D. Vernstrom, R. Atanasoski, A.K. Schmoeckel, M.K. Debe, J.R. Dahn, Electrochim. Acta **53**, 688 (2007)
19. R. Kötz, S. Stucki, Electrochim. Acta **31**, 1311 (1986)
20. J. Gaudet, A.C. Tavares, S. Trasatti, D. Guay, Chem. Mater. **17**, 1570 (2005)
21. C.P. De Pauli, S. Trasatti, J. Electroanal. Chem. **396**, 161 (1995)
22. A. Marshall, S. Sunde, M. Tsypkin, R. Tunold, Int. J. Hydrogen Energy **32**, 2320 (2007)
23. R.S. Yeo, J. Orehotsky, W. Visscher, S. Srinivasan, J. Electrochem. Soc. **128**, 1900 (1981)
24. K. Kadakia, M.K. Datta, O.I. Velikokhatnyi, P. Jampani, S.K. Park, P. Saha, J.A. Poston, A. Manivannan, P.N. Kumta, Int. J. Hydrogen Energy **37**, 3001 (2012)
25. C.C.L. McCrory, S. Jung, J.C. Peters, T.F. Jaramillo, J. Am. Chem. Soc. **135**, 16977 (2013)
26. J.M. Gregoire, C. Xiang, S. Mitrovic, X. Liu, M. Marcin, E.W. Cornell, J. Fan, J. Jin, J. Electrochem. Soc. **160**, F337 (2013)
27. J.M. Gregoire, C.X. Xiang, X.N. Liu, M. Marcin, J. Jin, Rev. Sci. Instrum. **84**, 024102 (2013)
28. J. Fan, S.W. Boettcher, G.D. Stucky, Chem. Mater. **18**, 6391 (2006)
29. X.N. Liu, Y. Shen, R.T. Yang, S.H. Zou, X.L. Ji, L. Shi, Y.C. Zhang, D.Y. Liu, L.P. Xiao, X.M. Zheng, S. Li, J. Fan, G.D. Stucky, Nano Lett. **12**, 5733 (2012)
30. J.M. Gregoire, M. Kostylev, M.E. Tague, P.F. Mutolo, R.B. van Dover, F.J. DiSalvo, H.D. Abruña, J. Electrochem. Soc. **156**, B160 (2009)
31. X. Li, Q. Chen, I. McCue, J. Snyder, P. Crozier, J. Erlebacher, K. Sieradzki, Nano Lett. **14**, 2569 (2014)
32. F.R. Nikkuni, E.A. Ticianelli, L. Dubau, M. Chatenet, Electrocatalysis **4**, 104 (2013)